Article:
Chen, L, Gelin, MF and Shalashilin, DV orcid.org/0000-0001-6104-1277 (2019) Dynamics of a one-dimensional Holstein polaron: The multiconfigurational Ehrenfest method. Journal of Chemical Physics, 151 (24). 244116. ISSN 0021-9606

https://doi.org/10.1063/1.5132341

Dynamics of a one-dimensional Holstein polaron: the multiconfigurational Ehrenfest method

Lipeng Chen[1] [a], Maxim F. Gelin[1], and Dmitrii V. Shalashilin[2]

[1] *Department of Chemistry, Technische Universität München, Garching D-85747, Germany*

[2] *School of Chemistry, University of Leeds, Leeds LS2 9JT, United Kingdom*

Abstract

We have extended the multiconfigurational Ehrenfest (MCE) approach to investigate the dynamics of a one-dimensional Holstein molecular crystal model. It has been shown that the extended MCE approach yields results in perfect agreement with benchmark calculations by the hierarchy equations of motion method. The accuracies of the MCE approach in describing the dynamical properties of the Holstein polaron over a wide range of exciton transfer integral and exciton-phonon coupling are carefully examined by a detailed comparison with the fully variational multiple Davydov D_2 ansatz. It is found that while the MCE approach and the multi-D_2 ansatz produce almost exactly the same results for small transfer integral, the results obtained by the multi-D_2 ansatz start to deviate from those by the MCE approach at longer times for large transfer integral. A large number of coherent state basis functions is required to characterize the delocalized features of the phonon wave function in the case of large transfer integral, which becomes computationally too demanding for the multi-D_2 ansatz. The MCE approach, on the other hand, uses hundreds to thousands of trajectory guided basis functions and converges very well, thus providing an effective tool for accurate, efficient simulation of polaron dynamics.

[a] Electronic address: chen0846.chen@tum.de

I. INTRODUCTION

Accurate simulations of coupled electron-nuclear dynamics are still a challenging task due to the so-called "curse of dimensionality": the size of the basis set scales exponentially with the number of degrees of freedom (DOFs). A particularly promising technique alleviating this computational bottleneck is based on the idea which expands the nuclear wave function as a linear combination of time-dependent Gaussian basis functions [1–3]. This idea can be traced back to the seminal work of Heller [3], who proposed to use frozen Gaussian (FG) coherent states (CSs) (Gaussian with a fixed width) to describe nuclear dynamics semiclassically. Various approaches using trajectory guided basis sets of frozen Gaussian CSs have been developed to provide powerful numerical tools for accurate simulations of multidimensional electron-nuclear dynamics. The method of multiple spawning (MS) [4–6] uses adaptive Gaussian basis sets to adequately treat nonadiabatic dynamics involving several coupled potential energy surfaces (PESs). When the wavepackets approach strong nonadiabatic coupling regimes, a process called spawning is utilized to generate more Gaussians on another PES. Because the Gaussians on two different PESs quickly become decoupled, the basis set must be continuously increased in order to follow the dynamics more accurately. The methods of variational Multiconfigurational Gaussians (vMCG) [7, 8] and Davydov ansatz (DA) [9–12], on the other hand, use a grid of trajectory guided FGs with both the trajectories of FGs and their amplitudes determined from the full variational principle. The Gaussian-based multiconfiguration time-dependent Hartree (G-MCTDH) method [13] uses conventional MCTDH basis functions to treat few most important modes, while the rest of modes are described by FGs. While those fully variational methods (vMCG, DA, G-MCTDH) can achieve formally exact descriptions of quantum dynamics of coupled electron-nuclear systems, they become rather expensive and suffer from numerical instabilities as the number of DOFs increases.

The method of coupled CS (CCS) developed by Shalashilin and Child [14–16] is somewhat between MS and fully variational methods. The CCS method describes the wavefunction on a basis of coherent states which are propagated using the Hamiltonian averaged over the Gaussians. This brings some quantum effects to CCS trajectories, and the CCS method is thus considerably more accurate than the semiclassical alternatives. Since the CCS trajectories are independent from each other, the CCS method requires much fewer computational

resources than fully variational methods. The CCS method has been successfully applied to many different multi-dimensional systems, 10D Henon-Heiles potentials [17], the Fermi-resonance and intra-molecular energy transfer in the CHD3 molecule [18], the modelling of the absorption spectrum of the 24D pyrazine model [19], the calculation of high-order harmonic generation spectra [20]. The fermion coupled coherent states (F-CCS) method was developed to simulate the double ionization of He in intense laser fields [21]. Quite recently, CCS method has been extended to simulate the quantum dynamics of indistinguishable bosons in the second-quantization formalism [22]. A further generalization of the CCS method, the multi-configurational Ehrenfest (MCE) method [23, 24], has been proposed to treat nonadiabatic dynamics involving two or several electronic PESs. In the MCE method, the wave function is represented by an ensemble of Ehrenfest trajectories guided by quantum averaged Hamiltonian, which can thus characterize the dynamics in the classically forbidden regions. The idea behind the MCE method is that in a multidimensional system the Ehrenfest trajectory is not far away from the variational trajectory used in the fully variational methods. Hence the utilization of an ensemble of Ehrenfest trajectories can in principle provide formally exact descriptions of quantum dynamics of multidimensional systems. Two versions of the MCE method have been proposed, the first version, MCEv1, was shown to be an efficient and numerically accurate method for the description of dynamics of high dimensional model systems. It was demonstrated that for the spin-boson model, the MCEv1 method with only 50-200 Ehrenfest configurations can yield results which are in good agreement with those calculations by multi-layer MCTDH (ML-MCTDH) [25] for up to 2000 DOFs [23]. The second version, MCEv2 was developed for the on-the-fly ab initio calculations of ultrafast nonadiabatic dynamics of photo-excited molecules [26–28].

In this paper, we extend the MCEv1 method to study polaron dynamics of the Holstein model. The Holstein molecular crystal model describes a lattice of two-level molecules interacting with a bath consisting of intra- and intermolecular vibrational modes. This model has been widely used to investigate the charge and energy transport in organic materials and natural light harvesting complexes [29, 30]. The dynamical properties of the Holstein polaron have been simulated previously by the dynamical mean-field theory [31], the continuous-time quantum Monte Carlo [32], the time-evolving block-decimation method [33], the variational exact diagonalization [34], and the Davydov ansatz [35, 36]. The purpose of this paper is to demonstrate that a fully trajectory based quantum method with simple Ehrenfest

trajectories can simulate dynamical properties of the Holstein polaron rather accurately. The rest of the paper is organized as follows. In Sec. II we introduce the model Hamiltonian and the MCEv1 method. In Sec. III, numerical results on the dynamical properties of the Holstein polaron are shown and discussed. Conclusions are drawn in Sec. IV.

II. THEORY

A. The Holstein model

We consider a one-dimensional ring consisting of N identical molecules, each described as a two level system coupled with a vibrational mode. The Hamiltonian of the one-dimensional Holstein molecular crystal model can be written as [37, 38]

$$\hat{H} = \sum_n \Omega_n(\mathbf{Q})\hat{a}_n^\dagger \hat{a}_n + \sum_{m\neq n} J_{m,n}(\mathbf{Q})\hat{a}_m^\dagger \hat{a}_n + \hat{H}_{\rm ph}, \tag{1}$$

where $\hat{a}_n^\dagger(\hat{a}_n)$ is the creation (annihilation) operator of an exciton, described as a two level system at the nth site. $\mathbf{Q}$ denotes the nuclear coordinates, and $\hat{H}_{\rm ph}$ is the bath (phonon) Hamiltonian. By adopting the Einstein phonons, $\hat{H}_{\rm ph}$ takes the form

$$\hat{H}_{\rm ph} = \omega_0 \sum_n \hat{b}_n^\dagger \hat{b}_n \tag{2}$$

where ω_0 is the dispersionless phonon frequency, and $\hat{b}_n^\dagger(\hat{b}_n)$ is the phonon creation (annihilation) operator for the nth site.

Taking a Taylor expansion of $\Omega_n(\mathbf{Q})$ and $J_{mn}(\mathbf{Q})$ to first order in nuclear coordinates $\mathbf{Q}$ and considering only nearest-neighbor coupling, one obtains

$$\hat{H} = \Omega \sum_n \hat{a}_n^\dagger \hat{a}_n - J \sum_n \hat{a}_n^\dagger(\hat{a}_{n+1} + \hat{a}_{n-1}) + \hat{H}_{\rm ph} + \hat{H}_{\rm ex-ph}^{\rm diag} + \hat{H}_{\rm ex-ph}^{\rm o.d.}, \tag{3}$$

where $\Omega = \Omega_n(\mathbf{Q}=\mathbf{0})$ is the site energy, J is the nearest-neighbor transfer integral $J_{m,n}(\mathbf{Q}=\mathbf{0}) = -J\delta_{m,n\pm1}$, and $\hat{H}_{\rm ex-ph}^{\rm diag}$ and $\hat{H}_{\rm ex-ph}^{\rm o.d.}$ are the diagonal and off-diagonal exciton-phonon coupling Hamiltonians, respectively,

$$\hat{H}_{\rm ex-ph}^{\rm diag} = -g\omega_0 \sum_n \hat{a}_n^\dagger \hat{a}_n(\hat{b}_n^\dagger + \hat{b}_n), \tag{4}$$

$$\hat{H}_{\rm ex-ph}^{\rm o.d.} = \frac{1}{2}\phi\omega_0 \sum_{n,l} \left[\hat{a}_n^\dagger \hat{a}_{n+1}\left(\hat{b}_l^\dagger + \hat{b}_l\right)(\delta_{n+1,l} - \delta_{n,l}) + \hat{a}_n^\dagger \hat{a}_{n-1}\left(\hat{b}_l^\dagger + \hat{b}_l\right)(\delta_{n,l} - \delta_{n-1,l})\right]. \tag{5}$$

The parameters g and ϕ are the diagonal and the off-diagonal exciton-phonon coupling strength, respectively. Since the exciton number operator $\hat{N}_{\rm ex} = \sum_n \hat{a}_n^\dagger \hat{a}_n$ commutes with the Hamiltonian $\hat{H}$, the first term ($\Omega \sum_n \hat{a}^\dagger \hat{a}_n$) of Eq. 3 is a constant operator which can be neglected. Thus the Hamiltonian $\hat{H}$ can be simplified as

$$\hat{H} = \hat{H}_{\rm ex} + \hat{H}_{\rm ph} + \hat{H}_{\rm ex-ph}^{\rm diag} + \hat{H}_{\rm ex-ph}^{\rm o.d.} \tag{6}$$

with a simplified form of the exciton Hamiltonian

$$\hat{H}_{\rm ex} = -J \sum_n \hat{a}_n^\dagger \left(\hat{a}_{n+1} + \hat{a}_{n-1}\right) \tag{7}$$

The phonon and exciton-phonon coupling Hamiltonians can be further written in the phonon momentum space as

$$\hat{H}_{\rm ph} = \sum_q \omega_q \hat{b}_q^\dagger \hat{b}_q, \tag{8}$$

$$\hat{H}_{\rm ex-ph}^{\rm diag} = -\frac{g}{\sqrt{N}} \sum_{n,q} \omega_q \hat{a}_n^\dagger \hat{a}_n \left(e^{iqn}\hat{b}_q + e^{-iqn}\hat{b}_q^\dagger\right), \tag{9}$$

$$\hat{H}_{\rm ex-ph}^{\rm o.d.} = \frac{\phi}{2\sqrt{N}} \sum_{n,q} \omega_q \left\{\hat{a}_n^\dagger \hat{a}_{n+1} \left[e^{iqn}(e^{iq}-1)\hat{b}_q + \text{H.c.}\right] + \hat{a}_n^\dagger \hat{a}_{n-1} \left[e^{iqn}(1-e^{-iq})\hat{b}_q + \text{H.c.}\right]\right\} \tag{10}$$

Here H.c. denotes the Hermitian conjugate, $\hat{b}_q^\dagger(\hat{b}_q)$ is the creation (annihilation) operator of a phonon with frequency ω_q

$$\hat{b}_q^\dagger = N^{-1/2} \sum_n e^{iqn} \hat{b}_n^\dagger, \quad \hat{b}_n^\dagger = N^{-1/2} \sum_q e^{-iqn} \hat{b}_q^\dagger \tag{11}$$

In this paper we parametrise the Holstein model in terms of the parameters of the phononic modes. We take $\omega_q = \omega_0 \left[1 + W\left(2|q|/\pi - 1\right)\right]$ as the dispersion relation for phonons, where $q = 2\pi l/N$ represents the phonon momentum index with $l = -\frac{N}{2} + 1, \cdots, \frac{N}{2}$. ω_0 is the central energy of the phonon band and is set to unity as the energy unit, W is the band width between 0 and 1.

B. The multi-configurational Ehrenfest method

In the MCEv1 method, the wave function can be written as a combination of M-configurations

$$|\Psi(t)\rangle = \sum_{k=1}^{M}\left(\sum_{n=1}^{N} a_{kn}(t)\hat{a}_n^\dagger|0\rangle_{\rm ex}\right)|\mathbf{z}_k(t)\rangle = \sum_{k=1}^{M}\left(\sum_{n=1}^{N} a_{kn}(t)\hat{a}_n^\dagger|0\rangle_{\rm ex}\right)\exp\left[\sum_q\left(z_{kq}\hat{b}_q^\dagger - z_{kq}^*\hat{b}_q\right)\right]|0\rangle_{\rm ph} \tag{12}$$

Here, a_{kn} and z_{kq} represent exciton amplitudes and phonon displacements, respectively. k and n are the configuration index and the site number in the molecular ring. The equations of motion for a set of wave function parameters a_{kn}, z_{kq} can be obtained from the Dirac-Frenkel time-dependent variational principles [39, 40]. The corresponding Lagrangian L is formulated as

$$\begin{aligned} L &= \langle\Psi|i\frac{\hat{\partial}}{\partial t} - \hat{H}|\Psi\rangle \\ &= \frac{i}{2}\sum_{k,j}^{M}\sum_{n}^{N}\Bigg\{\left[a_{kn}^*\dot{a}_{jn} - \dot{a}_{kn}^* a_{jn}\right] + a_{kn}^* a_{jn}\sum_q\left(\frac{z_{kq}\dot{z}_{kq}^* + \dot{z}_{kq}z_{kq}^* - z_{jq}\dot{z}_{jq}^* - \dot{z}_{jq}z_{jq}^*}{2} + z_{kq}^*\dot{z}_{jq} - z_{jq}\dot{z}_{kq}^*\right) \\ &\quad\Bigg\}R_{kj} - \langle\Psi|\hat{H}|\Psi\rangle \end{aligned} \tag{13}$$

with

$$R_{kj} = \langle\mathbf{z}_k|\mathbf{z}_j\rangle = \exp\left\{\sum_q z_{kq}^* z_{jq} - \frac{1}{2}\left(|z_{kq}|^2 + |z_{jq}|^2\right)\right\} \tag{14}$$

and

$$\langle\Psi|\hat{H}|\Psi\rangle = E_{\rm tot} = E_{\rm ex} + E_{\rm ph} + E_{\rm diag} + E_{\rm od} \tag{15}$$

$$E_{\rm ex} = \langle\Psi|\hat{H}_{\rm ex}|\Psi\rangle = -J\sum_{k,j}^{M}\sum_n a_{kn}^*\left(a_{j,n+1} + a_{j,n-1}\right)R_{kj} \tag{16}$$

$$E_{\rm ph} = \langle\Psi|\hat{H}_{\rm ph}|\Psi\rangle = \sum_{k,j}^{M}\sum_n a_{kn}^* a_{jn}\sum_q \omega_q z_{kq}^* z_{jq} R_{kj} \tag{17}$$

$$E_{\rm diag} = \langle\Psi|\hat{H}_{\rm ex-ph}^{\rm diag}|\Psi\rangle = -\frac{g}{\sqrt{N}}\sum_{k,j}^{M}\sum_n a_{kn}^* a_{jn}\sum_q \omega_q\left(e^{iqn}z_{jq} + e^{-iqn}z_{kq}^*\right)R_{kj} \tag{18}$$

$$\begin{aligned} E_{\rm od} = \langle\Psi|\hat{H}_{\rm ex-ph}^{\rm o.d.}|\Psi\rangle = \frac{\phi}{2\sqrt{N}}\sum_{k,j}^{M}\sum_n\sum_q \omega_q R_{kj}\Big\{&a_{kn}^* a_{j,n+1}\left[e^{iqn}(e^{iq}-1)z_{jq} + e^{-iqn}(e^{-iq}-1)z_{kq}^*\right] \\ &+ a_{kn}^* a_{j,n-1}\left[e^{iqn}(1-e^{-iq})z_{jq} + e^{-iqn}(1-e^{iq})z_{kq}^*\right]\Big\} \end{aligned} \tag{19}$$

Variation of the coefficient a_{kn} yields the equations of motion for a_{jn},

$$
\begin{aligned}
&\sum_j^M \left\{ i\dot{a}_{jn} + i a_{jn} \sum_q \left[z_{kq}^* \dot{z}_{jq} - \frac{\dot{z}_{jq} z_{jq}^* + z_{jq}\dot{z}_{jq}^*}{2} \right] \right\} R_{kj} \\
=&-J \sum_j^M \left(a_{j,n+1} + a_{j,n-1} \right) R_{kj} \\
+&\sum_j a_{jn} \sum_q \omega_q z_{kq}^* z_{jq} R_{kj} \\
-&\frac{g}{\sqrt{N}} \sum_j a_{jn} \sum_q \omega_q \left(e^{iqn} z_{jq} + e^{-iqn} z_{kq}^* \right) R_{kj} \\
+&\frac{\phi}{2\sqrt{N}} \sum_j a_{j,n+1} \sum_q \omega_q \left[e^{iqn}(e^{iq}-1) z_{jq} + e^{-iqn}(e^{-iq}-1) z_{kq}^* \right] R_{kj} \\
+&\frac{\phi}{2\sqrt{N}} \sum_j a_{j,n-1} \sum_q \omega_q \left[e^{iqn}(1-e^{-iq}) z_{jq} + e^{-iqn}(1-e^{iq}) z_{kq}^* \right] R_{kj}
\end{aligned} \tag{20}
$$

We can also apply the variational principle to $|\mathbf{z}_j\rangle$, yielding equations of motion for $|\mathbf{z}_j\rangle$ which is equivalent to those of fully variational methods. The equation of motion for $|\mathbf{z}_j\rangle$ can be explicitly derived as

$$
\begin{aligned}
&-i\sum_j^M \sum_n a_{kn}^* \dot{a}_{jn} z_{jq} R_{kj} - i \sum_j^M \sum_n a_{kn}^* a_{jn} \dot{z}_{jq} R_{kj} - \frac{i}{2} \sum_j^M \sum_n a_{kn}^* a_{jn} z_{jq} R_{kj} \sum_p \left(2 z_{kp}^* \dot{z}_{jp} - \dot{z}_{jp} z_{jp}^* - z_{jp} \dot{z}_{jp}^* \right) \\
&= J \sum_j^M \sum_n a_{kn}^* \left(a_{j,n+1} + a_{j,n-1} \right) z_{jq} R_{kj} - \sum_j^M \sum_n a_{kn}^* a_{jn} \left(\omega_q + \sum_p \omega_p z_{kp}^* z_{jp} \right) z_{jq} R_{kj} \\
&\quad + \frac{g}{\sqrt{N}} \sum_j^M \sum_n a_{kn}^* a_{jn} \omega_q e^{-iqn} R_{kj} + \frac{g}{\sqrt{N}} \sum_j^M \sum_n a_{kn}^* a_{jn} z_{jq} \sum_p \omega_p \left(e^{ipn} z_{jp} + e^{-ipn} z_{kp}^* \right) R_{kj} \\
&\quad - \frac{\phi}{2\sqrt{N}} \sum_j^M \sum_n \omega_q a_{kn}^* \left[a_{j,n+1} e^{-iqn}(e^{-iq}-1) + a_{j,n-1} e^{-iqn}(1-e^{iq}) \right] R_{kj} \\
&\quad - \frac{\phi}{2\sqrt{N}} \sum_j^M \sum_n \left(a_{k,n+1}^* a_{jn} + a_{kn}^* a_{j,n+1} \right) z_{jq} \sum_p \omega_p \left[e^{ipn}(e^{ip}-1) z_{jp} + e^{-ipn}(e^{-ip}-1) z_{kp}^* \right] R_{kj}
\end{aligned} \tag{21}
$$

Eqs (20) and (21) are the equations of motion for the Holstein polaron dynamcis with the multiple Davydov D_2 ansatz. In the MCEv1 method a simpler choice of trajectories is

made. Each $\mathbf{z}_j$ follows its own Ehrenfest equation [23]

$$\begin{aligned} i\dot{\mathbf{z}}_j &= \frac{\partial H_j^{\mathrm{Ehr}}}{\partial \mathbf{z}_j^*} \\ H_j^{\mathrm{Ehr}} &= \frac{\langle\Psi_j|\hat{H}|\Psi_j\rangle}{\langle\Psi_j|\Psi_j\rangle} \\ |\Psi_j\rangle &= \sum_n^N a_{jn}\hat{a}_n^\dagger|0\rangle_{\mathrm{ex}}|\mathbf{z}_j\rangle \end{aligned} \tag{22}$$

with

$$\begin{aligned} &\langle\Psi_j|\hat{H}|\Psi_j\rangle \\ =&-J\sum_n a_{jn}^*\left(a_{j,n+1}+a_{j,n-1}\right) \\ &+\sum_n a_{jn}^* a_{jn}\sum_q \omega_q z_{jq}^* z_{jq} \\ &-\frac{g}{\sqrt{N}}\sum_n a_{jn}^* a_{jn}\sum_q \omega_q\left(e^{iqn}z_{jq}+e^{-iqn}z_{jq}^*\right) \\ &+\frac{\phi}{2\sqrt{N}}\sum_n\sum_q \omega_q\Big\{a_{jn}^* a_{j,n+1}\left[e^{iqn}(e^{iq}-1)z_{jq}+e^{-iqn}(e^{-iq}-1)z_{jq}^*\right] \\ &+a_{jn}^* a_{j,n-1}\left[e^{iqn}(1-e^{-iq})z_{jq}+e^{-iqn}(1-e^{iq})z_{jq}^*\right]\Big\} \end{aligned} \tag{23}$$

and

$$\langle\Psi_j|\Psi_j\rangle = \sum_n a_{jn}^* a_{jn} \tag{24}$$

Finally we have the equation of motion for z_{jq} as follows

$$i\dot{z}_{jq} = \frac{\sum_n a_{jn}^* a_{jn}\omega_q(z_{jq}-\frac{g}{\sqrt{N}}e^{-iqn})+\frac{\phi}{2\sqrt{N}}\sum_n \omega_q e^{-iqn}\left(a_{jn}^* a_{j,n+1}(e^{-iq}-1)+a_{jn}^* a_{j,n-1}(1-e^{iq})\right)}{\sum_n a_{jn}^* a_{jn}} \tag{25}$$

The norm of the wave function can be calculated as

$$N(t) = \langle\Psi(t)|\Psi(t)\rangle = \sum_{k,j}^M\sum_n a_{kn}^* a_{jn} R_{kj} \tag{26}$$

Then the reduced single-exciton density matrix $\rho_{mn}(t)$ can be written as

$$\rho_{mn} = \langle\Psi(t)|\hat{a}_m^\dagger\hat{a}_n|\Psi(t)\rangle = \sum_{k,j}^M a_{km}^* a_{jn} R_{kj} \tag{27}$$

The exciton probability $P_{\rm ex}(t,n)$ and the phonon displacement $X_{\rm ph}(t,n)$ are usually used to characterize the dynamical properties of the Holstein polaron. The exciton probabilities $P_{\rm ex}(t,n) = \rho_{nn}(t)(n = 1, 2, \cdots, N)$ can be simply obtained from the diagonal elements of the reduced density matrix. The phonon displacement $X_{\rm ph}(t,n')$ in real space at the n'-th site is calculated by

$$\begin{aligned} X_{\rm ph}(t,n') &= \langle\Psi(t)|(\hat{b}_{n'} + \hat{b}^\dagger_{n'})|\Psi(t)\rangle \\ &= \frac{1}{\sqrt{N}}\langle\Psi(t)|\sum_q (e^{-iqn'}\hat{b}^\dagger_q + e^{iqn'}\hat{b}_q)|\Psi(t)\rangle \\ &= \frac{1}{\sqrt{N}}\sum_{kj}^{M}\sum_{n,q} a^*_{kn}a_{jn}R_{kj}\left[e^{-iqn'}z^*_{kq} + e^{iqn'}z_{jq}\right] \end{aligned} \tag{28}$$

The initial state of system is prepared to have one exciton on a single site i, and phonon modes are initially in the vacuum state, i.e., $|\Psi(0)\rangle = \hat{a}^\dagger_i|0\rangle_{\rm ex}|\mathbf{z}_0\rangle$, where $|\mathbf{z}_0\rangle = |\mathbf{0}\rangle_{\rm ph} = |00\cdots0\rangle_{\rm ph}$. Then a set of M CS basis functions $|\mathbf{z}_k\rangle(k = 1, \cdots, M)$ is selected to represent $|\mathbf{z}_0\rangle$. For this purpose, a uniformly distributed noise within the range $[-\epsilon, \epsilon]$ ($\epsilon = 10^{-12}$) is added to phonon displacements (both the real and imaginary part), and the quantum superposition sampling [41] is then used to determine the exciton amplitudes.

III. RESULTS AND DISCUSSION

We first compare results obtained by the MCEv1 method with benchmark calculations by the hierarchy equations of motion (HEOM) method [42]. Fig. 1 shows the time evolution of the exciton probability $P_{\rm ex}(t,n)$ for the cases of J=0.2, W=0.5, g=0.3, ϕ=0, N=10 (left column) and J=0.1, W=0, g=0, ϕ=0.3, N=10 (right column). For both cases, the MCEv1 results (with configuration $M = 400$) are in perfect agreement with the HEOM results (see Figs. 1(a-b) and (d-e)). The exciton probability difference $\Delta P_{\rm ex}(t,n)$ between two methods is found to be about four orders of magnitude smaller than the value of $P_{\rm ex}(t,n)$ (see Figs. 1(c,f)). It is worth mentioning that the comparisons between two methods are restricted to the small system size and weak exciton-phonon coupling strengths because the HEOM method becomes computationally unfeasible for systems of many two-level molecules which are moderately to strongly coupled to intra- and inter-molecular vibrational modes. Furthermore, the HEOM method is unable to capture explicit information on bosonic dynamics since the boson DOFs are traced out in reduced density matrix approaches. The wave

function propagation method, on the other hand, allows for exploration of boson dynamics of coupled electron-boson systems. The MCEv1 method, in particular, is demonstrated to yield accurate polaron dynamics of the Holstein model over broad parameter regimes ranging from weak to strong exciton-phonon couplings.

We then compare the exciton probability $P_{\rm ex}(t,n)$ and the phonon displacement $X_{\rm ph}(t,n)$ obtained from the MCEv1 method with those from the multiple Davydov D_2 ansatz [35]. It is noted that multi-D_2 ansatz is essentially the same as the ansatz used in the MCEv1 method (see Eq. 12), the number of Ehrenfest configurations M in the MCEv1 method is called the multiplicity M in the multi-D_2 ansatz. The only difference is that in the multi-D_2 ansatz, the variational principle is employed to obtain the coupled equations of motion of the variational parameters for both electronic and nuclear DOFs, while the equation of motion for nuclear part is determined by the Ehrenfest dynamics in the MCEv1 method (Eq. 25). Using a trajectory guided basis set rather than that of full variational principle results in a huge reduction of computational cost. The MCEv1 method uses hundreds to thousands of trajectories and can thus treat quantum dynamics of larger systems rather accurately.

Fig. 2 displays the time evolution of the exciton probability $P_{\rm ex}(t,n)$ (left column) and the phonon displacement $X_{\rm ph}(t,n)$ (right column) obtained with the MCEv1 method ($M = 800$) and the multi-D_2 ansatz ($M = 32$) for the weak diagonal exciton-phonon coupling $g = 0.4$. One can clearly observe that both methods produce nearly the same time-dependent $P_{\rm ex}(t,n)$ and $X_{\rm ph}(t,n)$. The differences $\Delta P_{\rm ex}(t,n)$ and $\Delta X_{\rm ph}(t,n)$ between the MCEv1 method and multi-D_2 ansatz are negligible, about four and three orders of magnitude smaller than the corresponding $P_{\rm ex}(t,n)$ and $X_{\rm ph}(t,n)$, respectively. The exciton wave packets propagate from the initial site $n = 0$ to the entire chain with the velocity $v \approx \omega_0/2\pi$, which triggers phonon deformations along the exciton path due to the exciton-phonon coupling. It is also found that a pair of localized phonon wave packets travel at group velocities $\pm v_q$ with $v_q = \partial\omega_q/\partial q = 2W$.

Fig. 3 illustrates the exciton probability $P_{\rm ex}(t,n)$ (left column) and the phonon displacement $X_{\rm ph}(t,n)$ (right column) obtained with the MCEv1 method ($M = 1000$) and the multi-D_2 ansatz ($M = 32$) for an intermediate diagonal coupling $g = 0.8$. Both methods yield almost the same exciton and phonon wave packets, showing that the exciton and center V-shaped phonon wave packets travel with the velocity $v \approx \omega_0/4\pi$ which are nearly half of those for the weak diagonal coupling $g = 0.4$, while the outer independent V-shaped

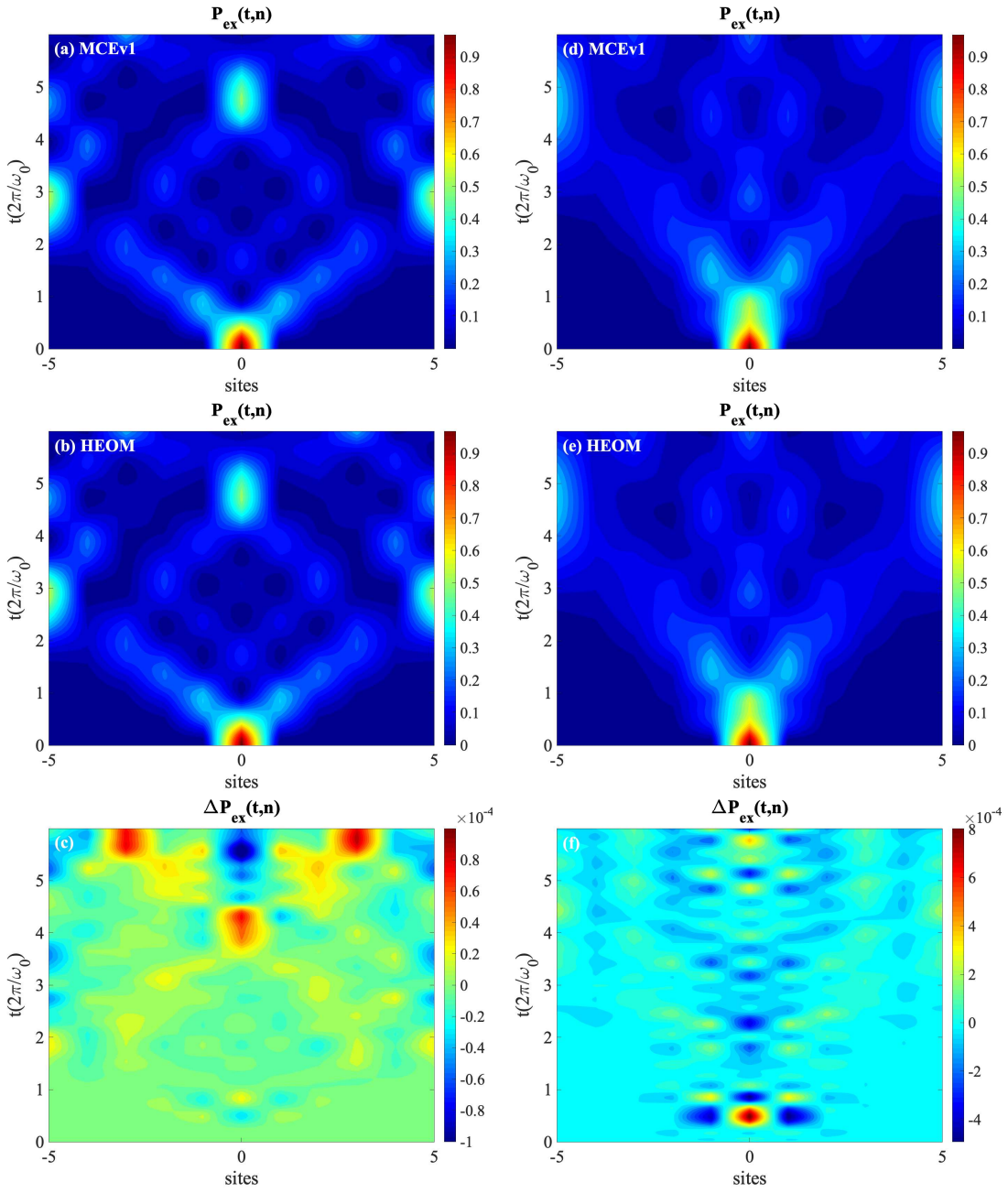

Figure 1. Time evolution of the exciton probability $P_{\mathrm{ex}}(t,n)$ for the cases of J=0.2, W=0.5, g=0.3, ϕ=0, N=10 (left column) and J=0.1, W=0, g=0, ϕ=0.3, N=10 (right column) obtained with the MCEv1 method (panels (a), (d), configuration $M = 400$) and the HEOM method (panels (b), (e)), respectively. The differences $\Delta P_{\mathrm{ex}}(t,n)$ between the HEOM method and the MCEv1 method are also displayed in panels (c,f).

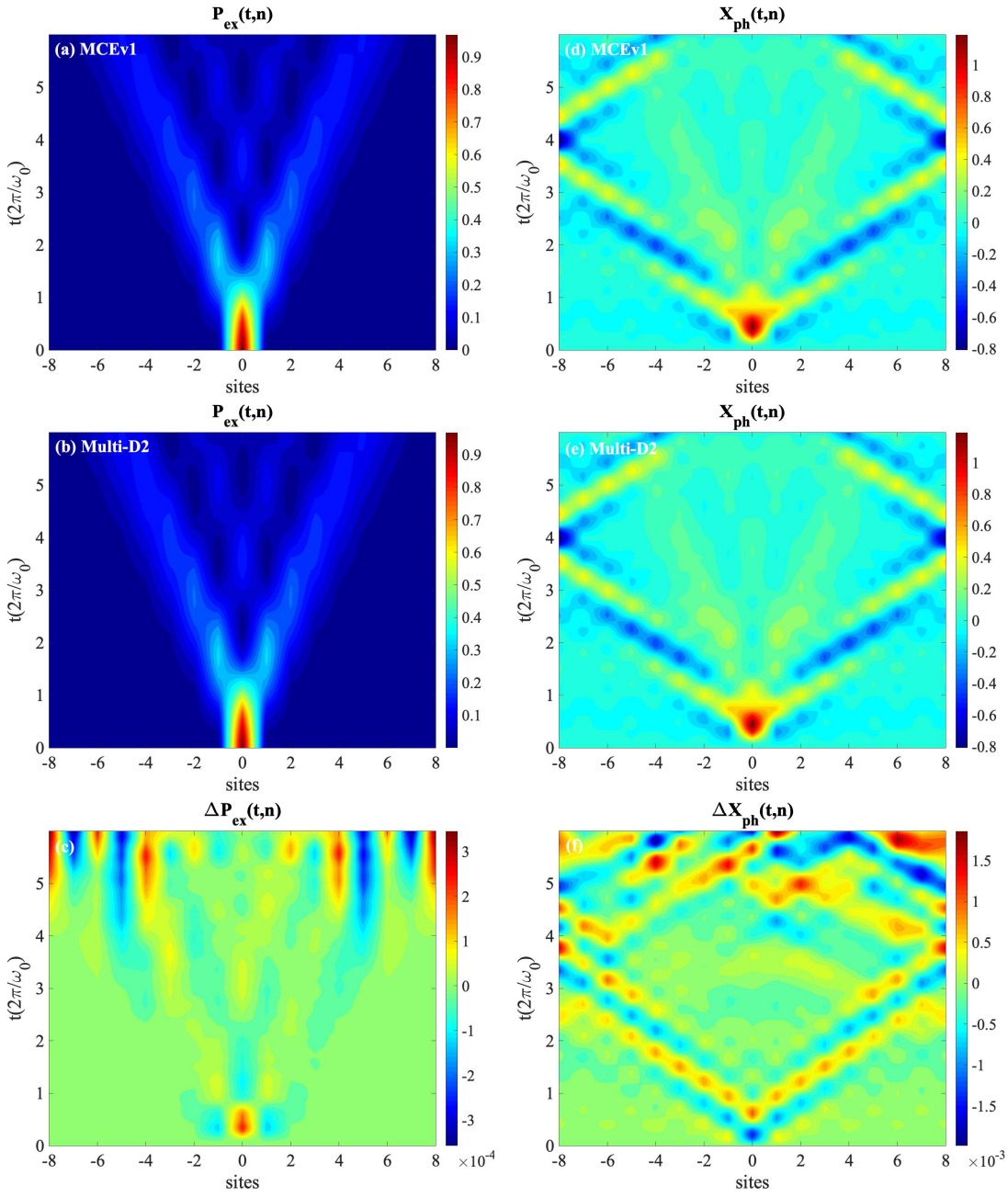

Figure 2. Time evolution of the exciton probability $P_{\rm ex}(t,n)$ (left column) and the phonon displacement $X_{\rm ph}(t,n)$ (right column) obtained with the MCEv1 method (panels (a), (d), configuration $M = 800$) and the multi-D_2 ansatz (panels (b), (e), multiplicity $M = 32$). The differences $\Delta P_{\rm ex}(t,n)$ and $\Delta X_{\rm ph}(t,n)$ between the MCEv1 method and multi-D_2 ansatz are also displayed in panels (c,f). The parameters are J=0.1, W=0.5, g=0.4, ϕ=0, N=16.

phonon wave packets are nearly unchanged. The differences $\Delta P_{\rm ex}(t,n)$ and $\Delta X_{\rm ph}(t,n)$ between the MCEv1 method and multi-D_2 ansatz are found to be about three and two orders of magnitude smaller than the corresponding $P_{\rm ex}(t,n)$ and $X_{\rm ph}(t,n)$, respectively.

The time evolution of the exciton probability $P_{\rm ex}(t,n)$ and the phonon displacement $X_{\rm ph}(t,n)$ obtained with the MCEv1 method ($M = 400$) and the multi-D_2 ansatz ($M = 32$) for the strong exciton-phonon coupling $g = 1.6$ are depicted in Fig. 4. Both methods capture the self-trapping features of polaron dynamics, illustrating that the exciton wavepackets as well as the phonon deformations induced by the strong exciton-phonon coupling are completely localized to the initial excitation site. It is shown again that the differences $\Delta P_{\rm ex}(t,n)$ and $\Delta X_{\rm ph}(t,n)$ are very small, about three and two orders of magnitude smaller than the corresponding $P_{\rm ex}(t,n)$ and $X_{\rm ph}(t,n)$, respectively.

The time evolutions of the exciton energy $E_{\rm ex}(t)$, the phonon energy $E_{\rm ph}(t)$, the exciton-phonon coupling energy $E_{\rm diag}(t)$ and the total energy $E_{\rm tot}(t)$ are plotted in Figs. 5(a-c), which correspond to the cases shown in Figs. 2-4, respectively. For all three cases, the energies obtained by multi-D_2 ansatz (open circles) are in perfect agreement with those obtained with the MCEv1 method (solid line).

The time evolution of the exciton probability $P_{\rm ex}(t,n)$ and the phonon displacement $X_{\rm ph}(t,n)$ obtained by the MCEv1 method and the multi-D_2 ansatz for three values of larger transfer integral $J = 0.2, 0.5, 0.8$ are displayed in Figs. 6-8. As shown in Fig. 6, both MCEv1 method ($M = 1000$) and the multi-D_2 ansatz ($M = 32$) provide accurate descriptions of polaron dynamics, yielding almost the same exciton probability and phonon displacement (see Figs. 6(c) and (f) for the differences $\Delta P_{ex}(t,n)$ and $\Delta X_{\rm ph}(t,n)$). As the transfer integral J is increased from 0.1 to 0.2, one can readily see that the exciton becomes more mobile because the propagation speed of the exciton is proportional to the exciton transfer integral J [43].

Fig. 7 illustrates the time evolution of the exciton probability $P_{\rm ex}(t,n)$ and the phonon displacement $X_{\rm ph}(t,n)$ at a larger transfer integral $J = 0.5$. It is found that a larger M is needed for both MCEv1 method ($M = 1400$) and multi-D_2 ansatz ($M = 56$) in order to accurately characterize the polaron dynamics. This is because a large transfer integral leads to a delocalized phonon wave function which is difficult to describe by the superposition of coherent states. As discussed in Ref. [35], the relative error (a quantity used to quantify the accuracy of a trial state) of the multi-D_2 ansatz monotonically increases

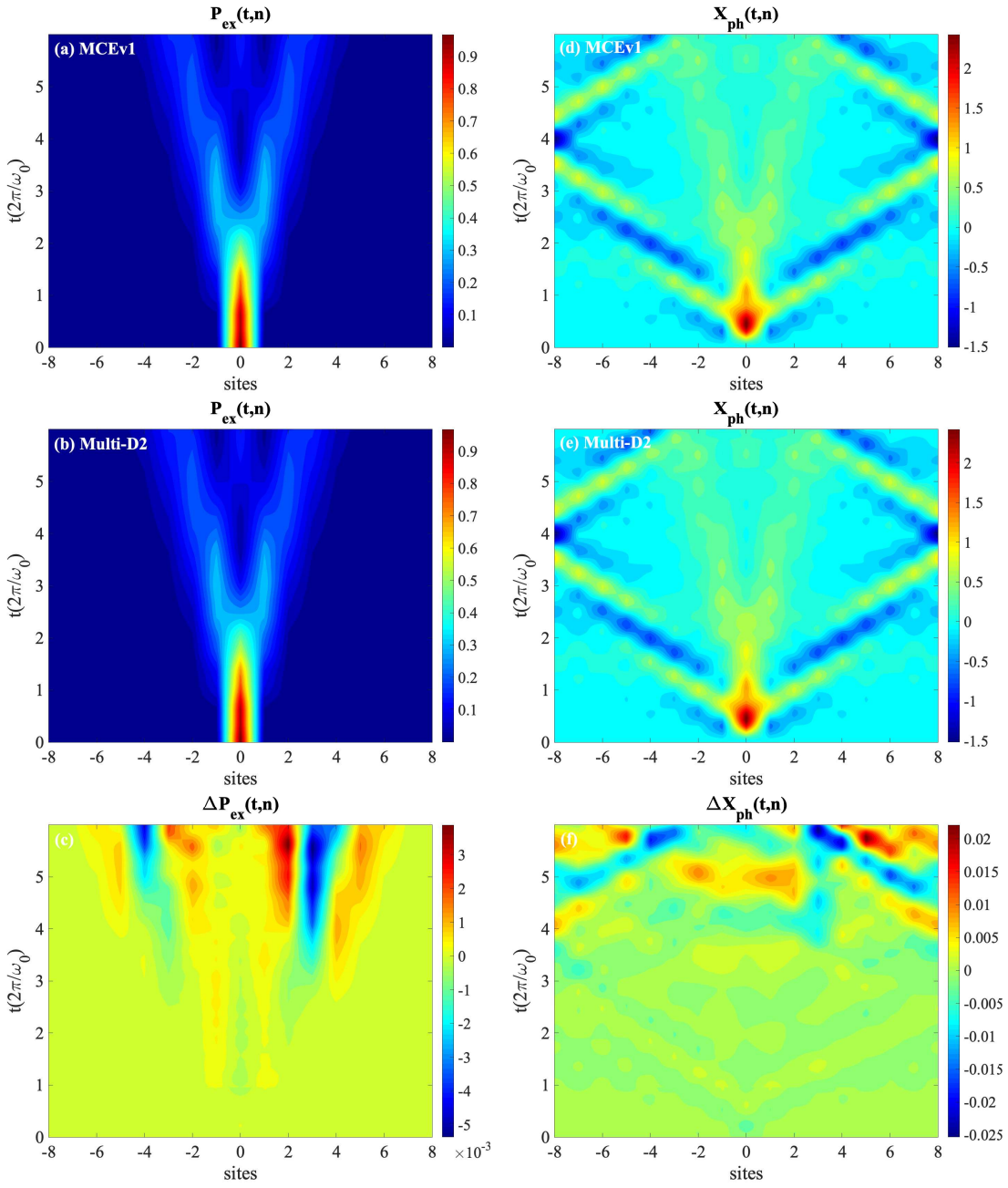

Figure 3. Time evolution of the exciton probability $P_{\rm ex}(t,n)$ (left column) and the phonon displacement $X_{\rm ph}(t,n)$ (right column) obtained with the MCEv1 method (panels (a), (d), configuration $M = 1000$) and the multi-D_2 ansatz (panels (b), (e), multiplicity $M = 32$). The differences $\Delta P_{\rm ex}(t,n)$ and $\Delta X_{\rm ph}(t,n)$ between the MCEv1 method and multi-D_2 ansatz are also displayed in panels (c,f). The parameters are J=0.1, W=0.5, g=0.8, ϕ=0, N=16.

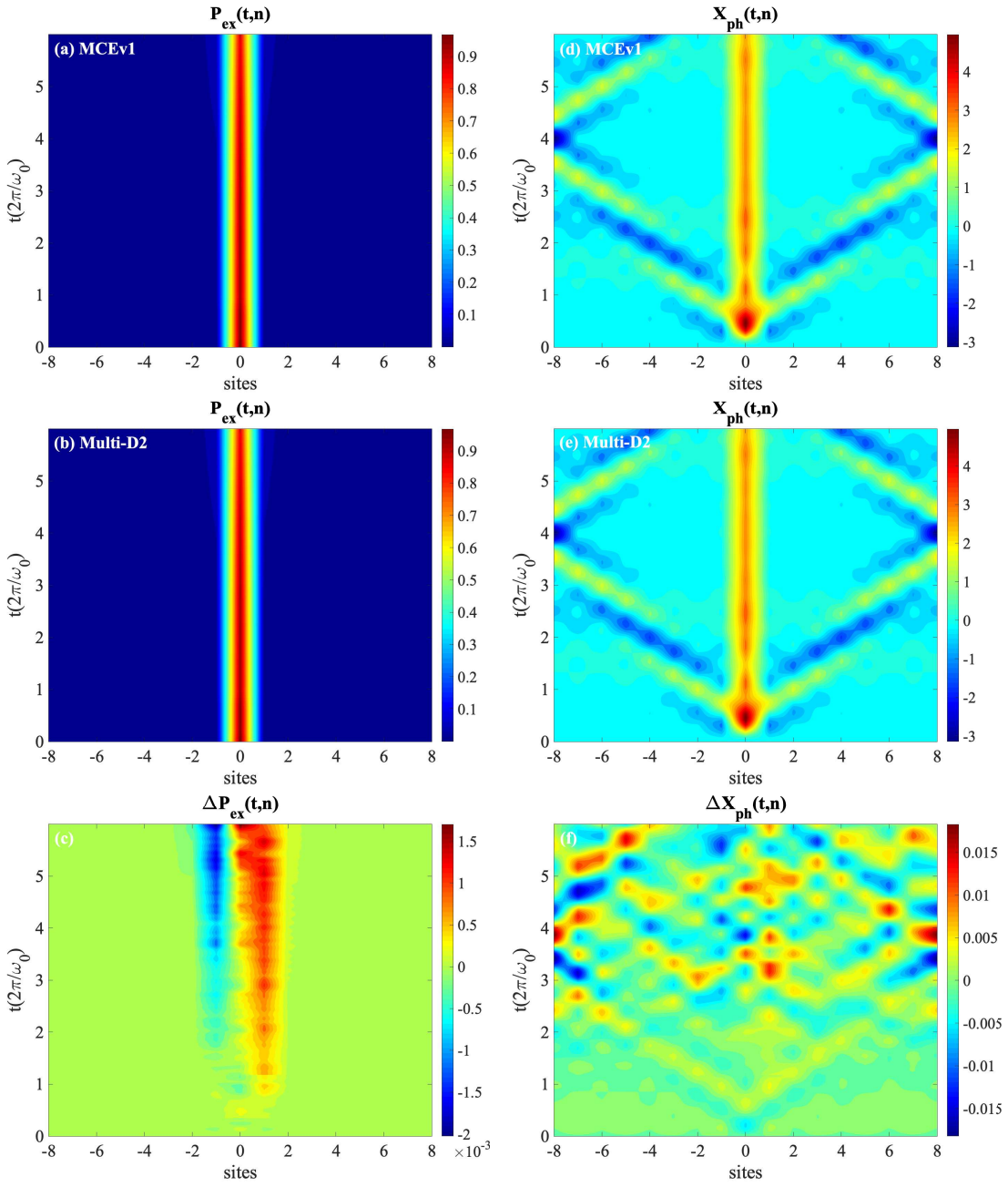

Figure 4. Time evolution of the exciton probability $P_{\mathrm{ex}}(t,n)$ (left column) and the phonon displacement $X_{\mathrm{ph}}(t,n)$ (right column) obtained with the MCEv1 method (panels (a), (d), configuration $M = 400$) and the multi-D_2 ansatz (panels (b), (e), multiplicity $M = 32$). The differences $\Delta P_{\mathrm{ex}}(t,n)$ and $\Delta X_{\mathrm{ph}}(t,n)$ between the MCEv1 method and multi-D_2 ansatz are also displayed in panels (c,f). The parameters are J=0.1, W=0.5, g=1.6, ϕ=0, N=16.

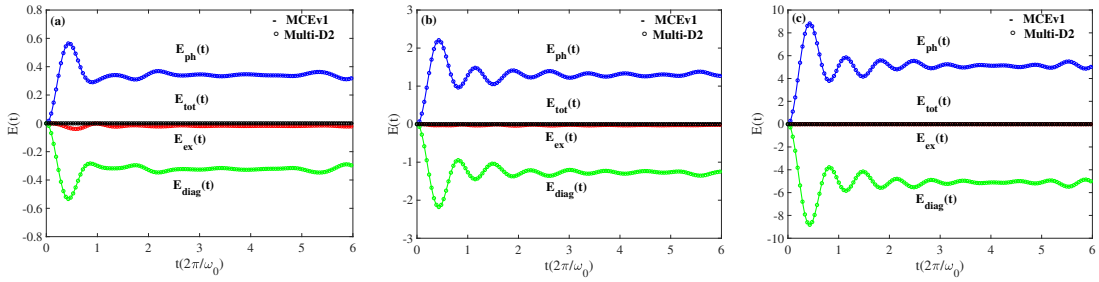

Figure 5. The time evolution of the exciton energy $E_{\rm ex}(t)$, the phonon energy $E_{\rm ph}(t)$, the exciton-phonon coupling energy $E_{\rm diag}(t)$ and the total energy $E_{\rm tot}(t)$ are displayed for J=0.1, W=0.5, g=0.4, ϕ=0, N=16 (a), J=0.1, W=0.5, g=0.8, ϕ=0, N=16 (b) and J=0.1, W=0.5, g=1.6, ϕ=0, N=16 (c), which correspond to the cases shown in Figs. 2-4, respectively. The solid line and open circles correspond to results obtained with the MCEv1 method and the multi-D_2 ansatz, respectively.

with the transfer integral J. Furthermore, like many fully variational methods, the multi-D_2 ansatz is known to suffer from numerical instabilities for a large M. This problem can be solved by pseudo-inverse of the coefficient matrix using the singular value decomposition during the numerical integration of the differential equations. However, computing a pseudo-inverse of a large matrix is computationally very demanding, which restricts the multiplicity M to a relatively small value. The MCEv1 method, on the other hand, can use hundreds to thousands of trajectories to capture the accurate dynamical properties of the Holstein polaron for large transfer integral J. As shown in Figs. 7 (c) and (f), the exciton probability and the phonon displacement calculated by multi-D_2 ansatz start to deviate slightly from those by the MCEv1 method after $t/(2\pi/\omega_0) > 3$.

The time evolution of the exciton probability $P_{\rm ex}(t,n)$ and the phonon displacement $X_{\rm ph}(t,n)$ at an even larger transfer integral $J = 0.8$ are shown in Fig. 8. It is well known that the systems with large transfer integral pose a challenging case for the multi-D_2 ansatz [35] as is clearly demonstrated in Figs. 8(c) and 8(f). One can readily see that the differences $\Delta P_{\rm ex}(t,n)$ and $\Delta X_{\rm ph}(t,n)$ between the multi-D_2 ansatz ($M = 56$) and the MCEv1 method ($M = 1600$) become relatively large as compared to the value of $P_{\rm ex}(t,n)$ and $X_{\rm ph}(t,n)$ after $t/(2\pi/\omega_0) > 3$. Nevertheless, the overall agreement between the multi-D_2 ansatz and the MCEv1 method is satisfactory.

The system energies, including the exciton energy $E_{\rm ex}$, the phonon energy $E_{\rm ph}$, the

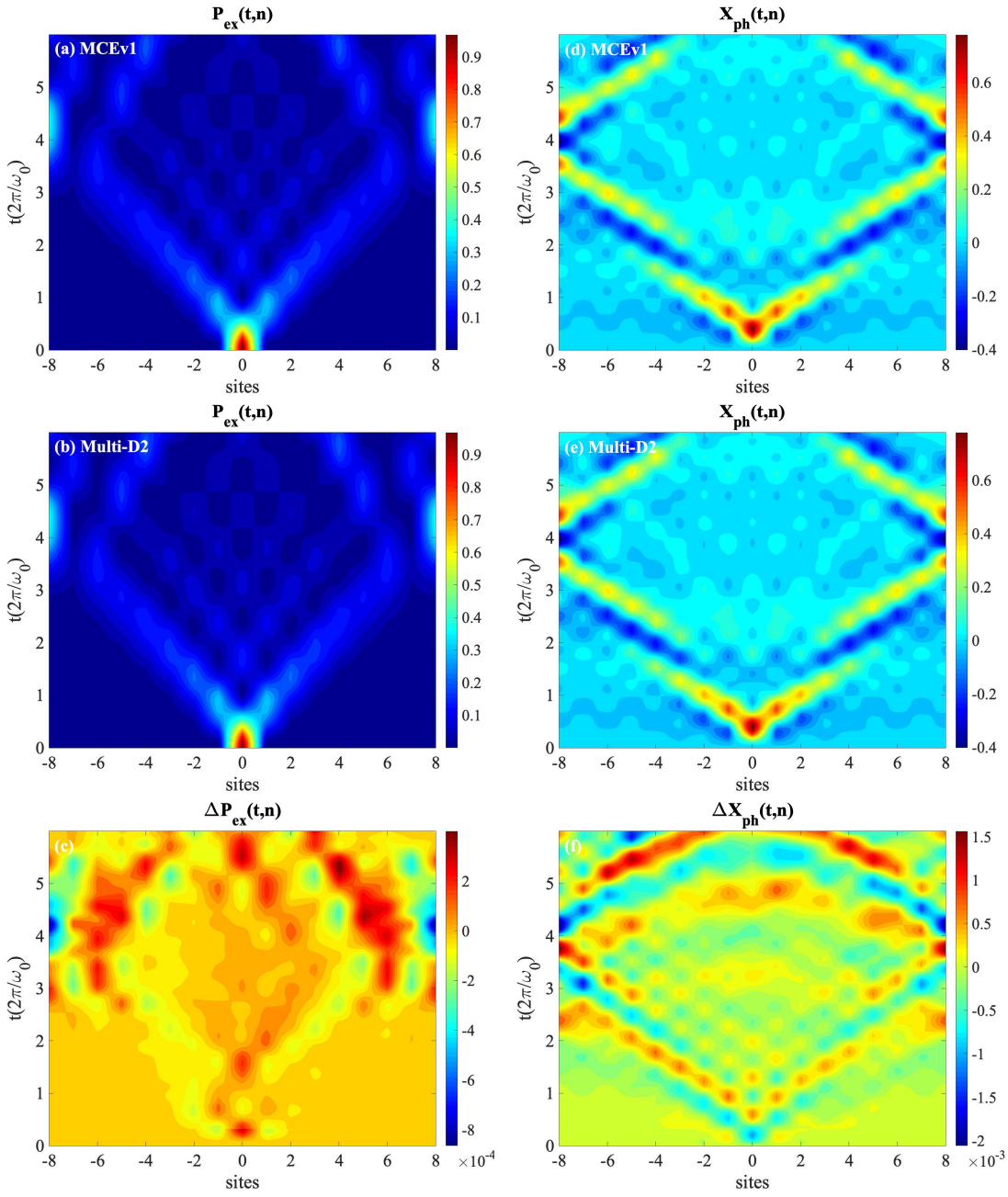

Figure 6. Time evolution of the exciton probability $P_{\mathrm{ex}}(t,n)$ (left column) and the phonon displacement $X_{\mathrm{ph}}(t,n)$ (right column) obtained with the MCEv1 method (panels (a), (d), configuration $M = 1000$) and the multi-D_2 ansatz (panels (b), (e), multiplicity $M = 32$). The differences $\Delta P_{\mathrm{ex}}(t,n)$ and $\Delta X_{\mathrm{ph}}(t,n)$ between the MCEv1 method and multi-D_2 ansatz are also displayed in panels (c,f). The parameters are J=0.2, W=0.5, g=0.3, ϕ=0, N=16.

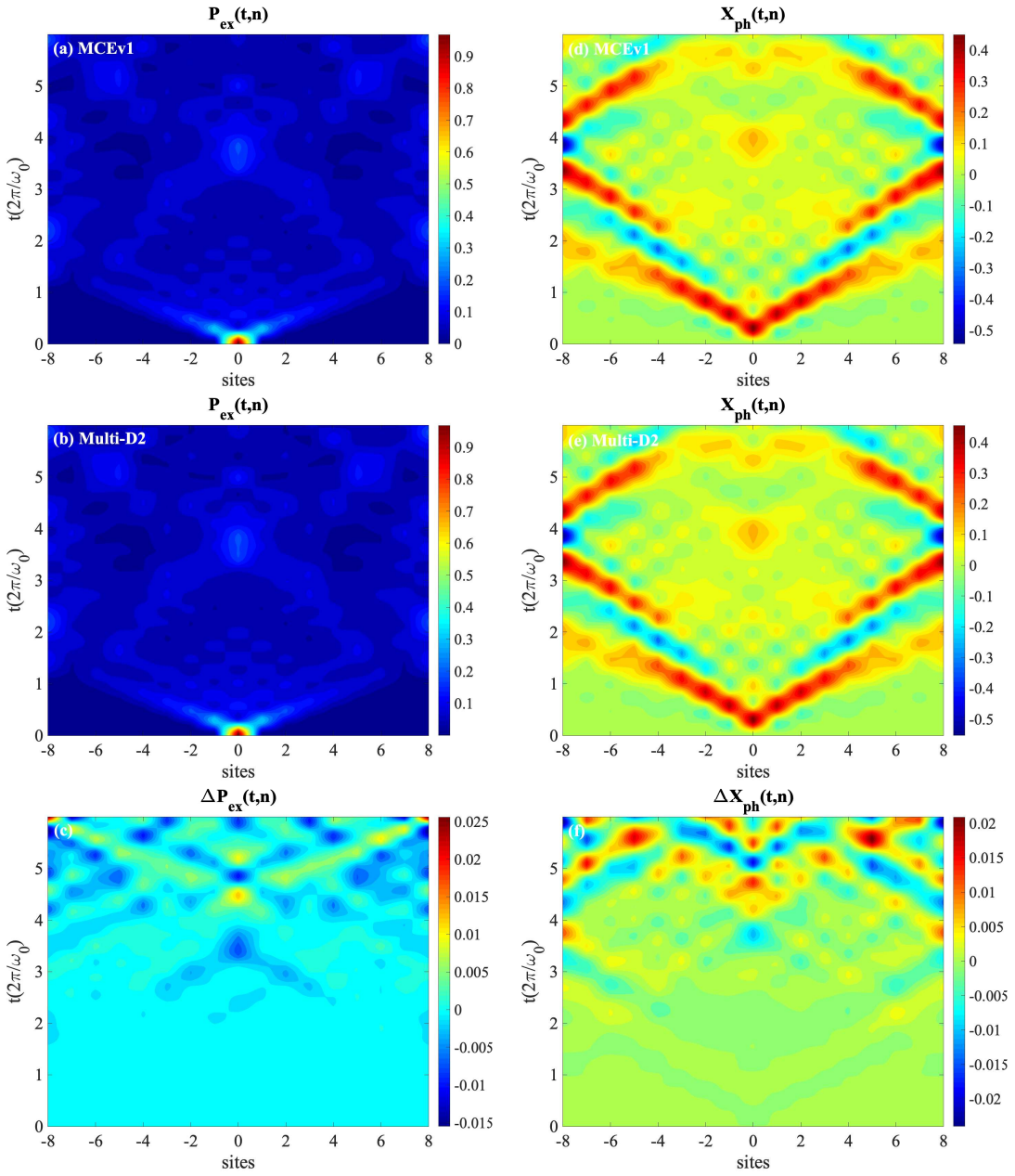

Figure 7. Time evolution of the exciton probability $P_{\rm ex}(t,n)$ (left column) and the phonon displacement $X_{\rm ph}(t,n)$ (right column) obtained with the MCEv1 method (panels (a), (d), configuration $M = 1400$) and the multi-D_2 ansatz (panels (b), (e), multiplicity $M = 56$). The differences $\Delta P_{\rm ex}(t,n)$ and $\Delta X_{\rm ph}(t,n)$ between the MCEv1 method and multi-D_2 ansatz are also displayed in panels (c,f). The parameters are J=0.5, W=0.5, g=0.3, ϕ=0, N=16.

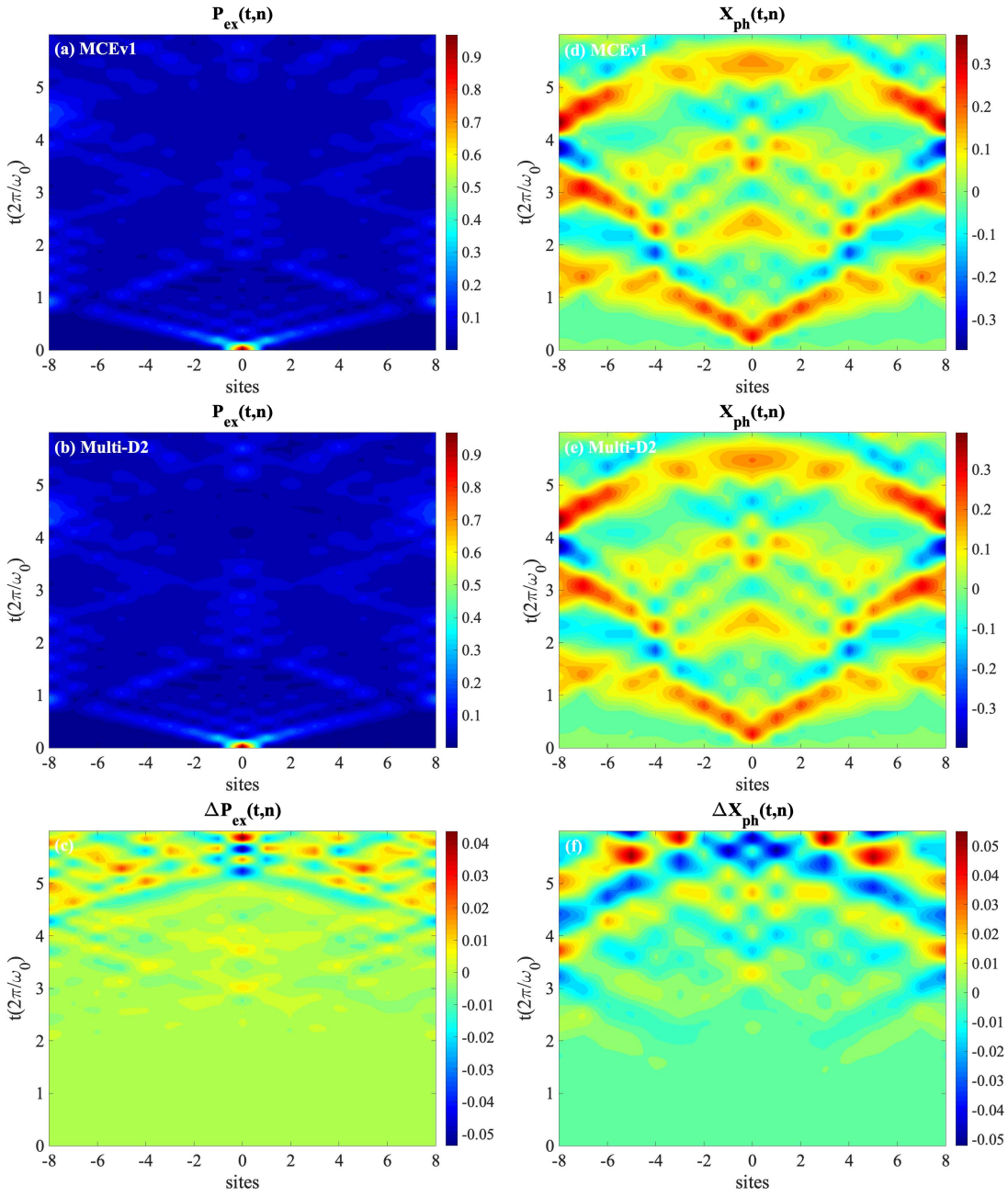

Figure 8. Time evolution of the exciton probability $P_{\rm ex}(t,n)$ (left column) and the phonon displacement $X_{\rm ph}(t,n)$ (right column) obtained with the MCEv1 method (panels (a), (d), configuration $M = 1600$) and the multi-D_2 ansatz (panels (b), (e), multiplicity $M = 56$). The differences $\Delta P_{\rm ex}(t,n)$ and $\Delta X_{\rm ph}(t,n)$ between the MCEv1 method and multi-D_2 ansatz are also displayed in panels (c,f). The parameters are J=0.8, W=0.5, g=0.3, ϕ=0, N=16.

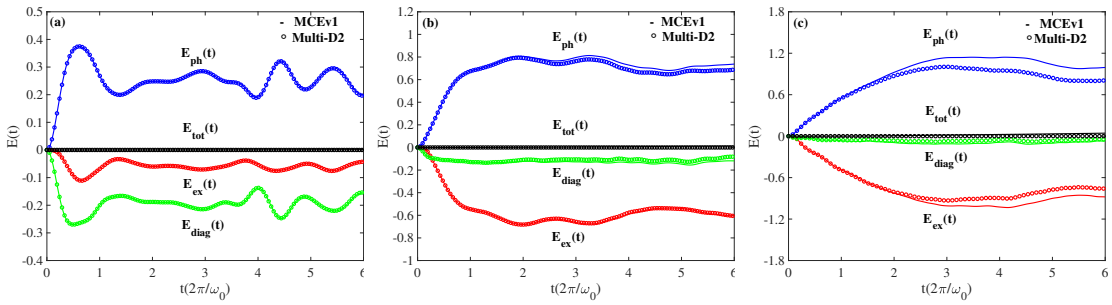

Figure 9. The time evolution of the exciton energy $E_{\rm ex}(t)$, the phonon energy $E_{\rm ph}(t)$, the exciton-phonon coupling energy $E_{\rm diag}(t)$ and the total energy $E_{\rm tot}(t)$ are displayed for J=0.2, W=0.5, g=0.3, ϕ=0, N=16 (a), J=0.5, W=0.5, g=0.3, ϕ=0, N=16 (b) and J=0.8, W=0.5, g=0.3, ϕ=0, N=16 (c), which correspond to the cases shown in Figs. 6-8, respectively. The solid line and open circles correspond to results obtained with the MCEv1 method and the multi-D_2 ansatz, respectively.

exciton-phonon coupling energy $E_{\rm diag}$ and the total energy $E_{\rm tot}$ for three values of the transfer integral, J=0.2, 0.5, 0.8 are plotted in Fig. 9, which correspond to the cases shown in Figs. 6-8. It is found that the energies calculated by the multi-D_2 ansatz match perfectly those calculated by the MCEv1 method for the case of $J = 0.2$, while the disparity of the energies calculated by the multi-D_2 ansatz and the MCEv1 method starts to emerge after $t/(2\pi/\omega_0) > 3$ for the case of $J = 0.5$ and becomes relatively large for the case of $J = 0.8$.

Fig. 10 illustrates the convergence with regard to the number of configurations used in the MCEv1 method for the challenging case of J=0.8, W=0.5, g=0.3, ϕ=0, N=16 (see Figs. 8 and 9(c)). The time evolution of the exciton $P_{\rm ex}(t, n)$ with $n = 0$ (left panel) and the phonon energy $E_{\rm ph}(t)$ (right panel) calculated by the MCEv1 method (with configuration M =1, 200, 600, 1200, 1600) are compared with those by the multi-D_2 ansatz (with multiplicity $M = 56$). It should be noted that MCEv1 with $M = 1$ (the Ehrenfest method) is equivalent to the variational method with the single D_2 ansatz [44]. It is found that the accuracy of the MCEv1 method is significantly enhanced with M, and the results obtained by the MCEv1 method with configuration $M = 200$ are close to those of the multi-D_2 ansatz with multiplicity $M = 56$. As the configuration M used in the MCEv1 method increases, both $P_{\rm ex}(t, 0)$ and $E_{\rm ph}(t)$ gradually converge to the exact results. This means that the multi-D_2 ansatz with M=56 is not fully converged, but increasing M would be computationally demanding. On the other hand, the MCEv1 method can afford larger basis set size and full

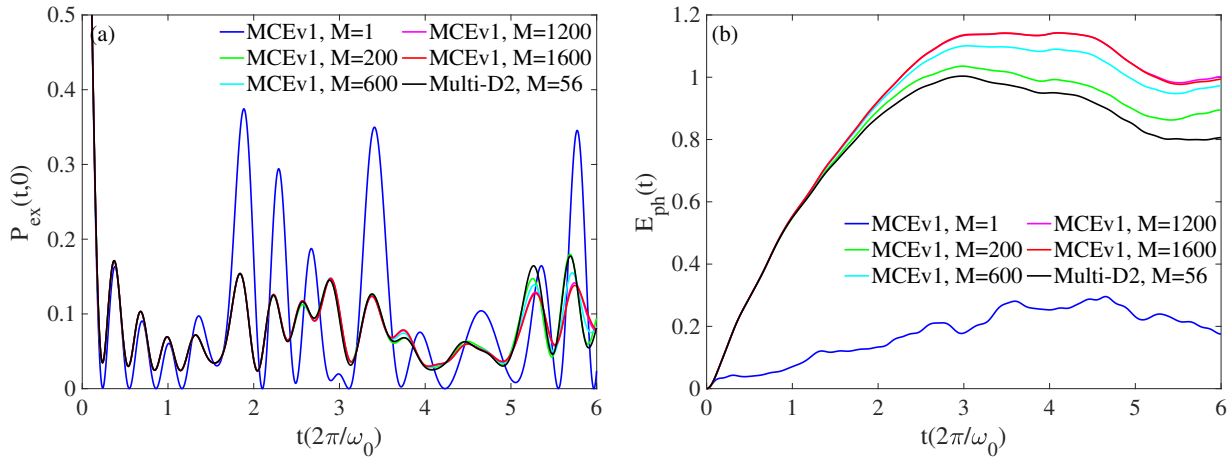

Figure 10. Time evolution of the exciton probability $P_{\rm ex}(t,n)$ with $n=0$ (left panel) and the phonon energy $E_{\rm ph}(t)$ (right panel) obtained with the MCEv1 method (with configuration $M=1,200,600,1200,1600$) and the multi-D_2 ansatz (with multiplicity $M=56$). The parameters are J=0.8, W=0.5, g=0.3, ϕ=0, N=16.

convergence can be achieved.

Fig. 11 displays the time evolution of the exciton probability $P_{\rm ex}(t,n)$ and the phonon displacement $X_{\rm ph}(t,n)$ calculated by the MCEv1 method ($M=1400$) and the multi-D_2 ansatz ($M=44$) for the off-diagonal coupling case of J=0.1, W=0.0, g=0.0, ϕ=0.4, N=16. It is found that the exciton is self-trapped in the initial site during the first phonon period $t<2\pi/\omega_0$, and correspondingly, there is minor lattice distortions in this time period regime. Then the exciton starts to spread over the molecular ring with the velocity $v\approx\omega_0/\pi$ due to the combined effect of the transfer integral and the off-diagonal exciton-phonon coupling. Both MCEv1 method and multi-D_2 ansatz reproduce the accurate dynamical properties of the Holstein polaron for the off-diagonal coupling case, and the agreement between them is quite good. This is also reflected in the Fig. 12 where the system energies calculated by the multi-D_2 are in very good agreement with those calculated by the MCEv1 method except the minor deviations at longer times.

IV. CONCLUSIONS

In summary, we have extended the MCEv1 method to study the polaron dynamics of the Holstein molecular crystal model. The validity of the method has been checked by comparing

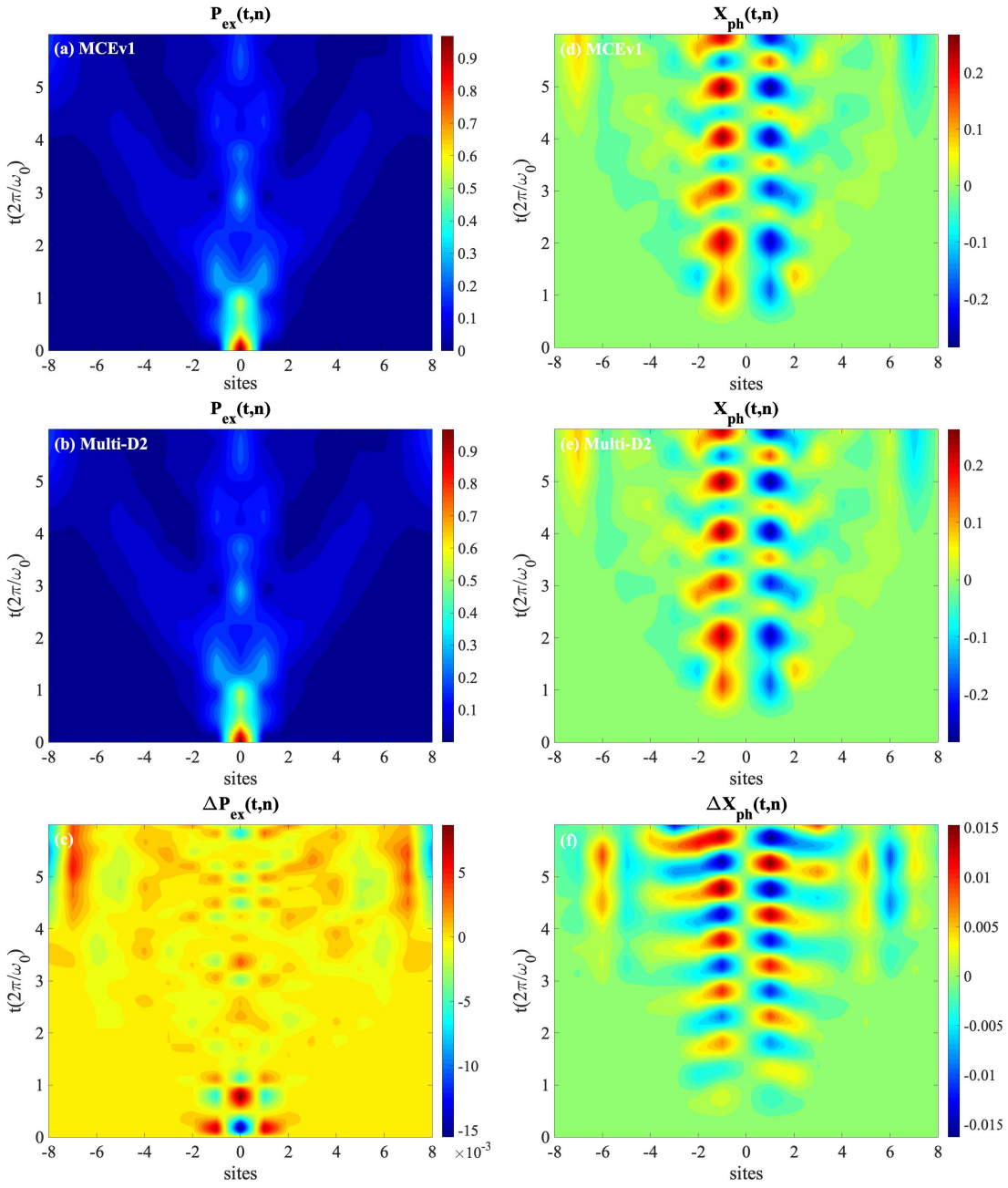

Figure 11. Time evolution of the exciton probability $P_{\mathrm{ex}}(t,n)$ (left column) and the phonon displacement $X_{\mathrm{ph}}(t,n)$ (right column) obtained with the MCEv1 method (panels (a), (d), configuration $M = 1400$) and the multi-D_2 ansatz (panels (b), (e), multiplicity $M = 44$). The differences $\Delta P_{\mathrm{ex}}(t,n)$ and $\Delta X_{\mathrm{ph}}(t,n)$ between the MCEv1 method and multi-D_2 ansatz are also displayed in panels (c,f). The parameters are J=0.1, W=0.0, g=0.0, ϕ=0.4, N=16.

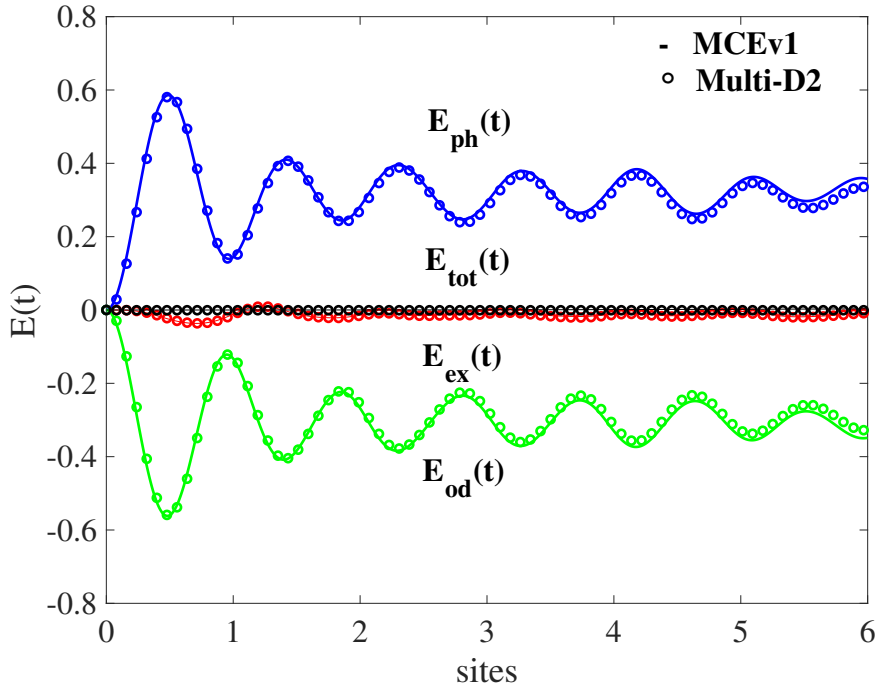

Figure 12. The time evolution of the exciton energy $E_{\rm ex}(t)$, the phonon energy $E_{\rm ph}(t)$, the exciton-phonon coupling energy $E_{\rm od}(t)$ and the total energy $E_{\rm tot}(t)$ are displayed for J=0.1, W=0.0, g=0.0, ϕ=0.4, N=16, which correspond to the case shown in Fig. 10. The solid line and open circles correspond to the results obtained with the MCEv1 method and the multi-D_2 ansatz, respectively.

the computed exciton probability with benchmark results from the hierarchy equations of motion approach, demonstrating that the MCEv1 method can provide numerically accurate and computationally efficient descriptions of polaron dynamics in the presence of diagonal and off-diagonal exciton-phonon couplings. The accuracies of the MCEv1 method in characterizing the dynamical properties of the Holstein polaron over a wide range of exciton transfer integral and exciton-phonon coupling strength are carefully examined by comparing with the fully variational multi-D_2 ansatz. It is found that both methods produce quite accurate exciton probability, phonon displacement as well as system energies over a broad range of diagonal exciton-phonon couplings for a small transfer integral. As the transfer integral increases, a larger number of CS basis functions is required to obtain numerically accurate results due to the delocalized features of the phonon wave function. However, increasing the basis size is computationally too demanding for the multi-D_2 ansatz since the numerical integration of differential equations involves the pseudo-inverse of the large coefficient matrix,

which restricts the number of CS basis functions to a relatively small value. On the other hand, the equations of motion of the CS basis are determined by the Ehrenfest dynamics in the MCEv1 method, leading to huge savings in computational costs. The MCEv1 method can thus use hundreds to thousands of trajectories to yield correct dynamical properties of the Holstein polaron for large transfer integral. While both methods give very accurate polaron dynamics at short times, the results obtained by the multi-D_2 ansatz are not easy to converge and they start deviating from those of the MCEv1 method at longer times for the case of large transfer integral. For the off-diagonal exciton-phonon coupling considered here, both MCEv1 method and multi-D_2 ansatz are shown to be capable of depicting the accurate dynamical properties of the Holstein polaron.

It is straightforward to extend the MCEv1 method to study the drift of charge carriers in an external electric field by employing a Holstein model with a phase-factor modified transfer integral [34, 45]. The concept of the polaron states (the quantum mixture of the exciton and intramolecular vibrational modes) is also important to explain the mechanism of the singlet fission processes in organic crystal materials [46–48]. In addition, recent experiments in cavity quantum electrodynamics (QED) have pointed to the importance of the polariton states (quantum mechanically mixed atomic and photonic states) in the descriptions of the strong light-matter interaction. The MCEv1 method can be straightforwardly extended to investigate those processes. Finally, it is also of great interest to integrate the MCEv1 method into the nonlinear response function formalism to simulate third-order spectroscopic signals [49–51]. Work in these directions is in progress.

ACKNOWLEDGMENTS

L. P. C. acknowledges support by a postdoctoral fellowship of the Alexander von Humboldt Foundation. M. F. G. acknowledges support from the Deutsche Forschungsgemeinschaft through a research grant and through the DFG Cluster of Excellence Munich-Centre for Advanced Photonics (http://www.munich-photonics.de). D.S. acknowledges EPSRC grant EP/P021123/1.

[1] E. J. Heller, J. Chem. Phys. **62**, 1544 (1975).

[2] E. J. Heller, Acc. Chem. Res. **14**, 368 (1981).

[3] E. J. Heller, J. Chem. Phys. **75**, 2923 (1981).

[4] M. Ben-Nun, T. J. Martinez, J. Chem. Phys. **112**, 6113 (2000).

[5] M. Ben-Nun, T. J. Martinez, Adv. Chem. Phys. **121**, 439 (2002).

[6] B. F. E. Curchod, T. J. Martinez, Chem. Rev. **118**, 3305 (2018).

[7] I. Burghardt, H. D. Meyer, and L. S. Cederbaum, J. Chem. Phys. **111**, 2927 (1999).

[8] G. A. Worth and I. Burghardt, Chem. Phys. Lett. **368**, 502 (2003).

[9] L. Chen, R. Borrelli, Y. Zhao, J. Phys. Chem. A. **121**, 8757 (2017).

[10] L. Chen, Y. Zhao, J. Chem. Phys. **147**, 214102 (2017).

[11] L. Chen, M. F. Gelin, Y. Zhao, Chem. Phys. **515**, 108 (2018).

[12] L. Chen, M. F. Gelin, W. Domcke, J. Chem. Phys. **150**, 024101 (2019).

[13] I. Burghardt, K. Giri, and G. A. Worth, J. Chem. Phys. **129**, 174104 (2008).

[14] D. V. Shalashilin, M. S. Child, J. Chem. Phys. **113**, 10028 (2000); **114**, 9296 (2001); **115**, 5367 (2001).

[15] D. V. Shalashilin, M. S. Child, Chem. Phys. **304**, 103 (2004).

[16] D. V. Shalashilin, M. S. Child, J. Chem. Phys. **121**, 3563 (2004).

[17] D. V. Shalashilin, M. S. Child, J. Chem. Phys. **128**, 054102 (2008).

[18] D. V. Shalashilin, M. S. Child, J. Chem. Phys. **119**, 1961 (2003).

[19] D. V. Shalashilin, M. S. Child, J. Chem. Phys. **121**, 3563 (2004).

[20] C. Symonds, J. Wu, M. Ronto, C. Zagoya, C. F. de Morisson Faria, D. V. Shalashilin, Phys. Rev. A. **91**, 023427 (2015).

[21] A. Kirrander, D. V. Shalashilin, Phys. Rev. A. **84**, 033406 (2011).

[22] J. A. Green, D. V. Shalashilin, Phys. Rev. A. **100**, 013607 (2019).

[23] D. V. Shalashilin, J. Chem. Phys. **130**, 244101 (2009).

[24] D. V. Shalashilin, J. Chem. Phys. **132**, 244111 (2010).

[25] H. Wang, M. Thoss, J. Chem. Phys. **119**, 1289 (2003).

[26] K. Saita, D. V. Shalashilin, J. Chem. Phys. **137**, 22A506 (2012).

[27] D. V. Makhov, W. J. Glover, T. J. Martinez, D. V. Shalashilin, J. Chem. Phys. **141**, 054110 (2014).

[28] D. V. Makhov, C. Symonds, S. F. Alberti, D. V. Shalashilin, Chem. Phys. **493**, 200 (2017).

[29] L. P. Chen, P. Shenai, F. L. Zheng, A. Somoza, Y. Zhao, Molecules, **20**, 15224 (2015).

[30] V. May, O. Kühn. *Charge and Energy Transfer Dynamics in Molecular Systems*, Wiley-VCH, Berlin, 2004.

[31] Y. Murakami, P. Werner, N. Tsuji, and H. Aoki, Phys. Rev. B. **91**, 045128 (2015).

[32] M. Hohenadler, Phys. Rev. B. **88**, 064303 (2013).

[33] F. Dorfner, L. Vidmar, C. Brockt, E. Jeckelmann, F. H. Meisner, Phys. Rev. B. **91**, 104302 (2015).

[34] L. Vidmar, J. Bonca, M. Mierzejewski, P. Prelovsek, and S. A. Trugman, Phys. Rev. B. **83**, 134301 (2011)

[35] N. Zhou, Z. Huang, J. Zhu, V. Chernyak, Y. Zhao, J. Chem. Phys. **143**, 014113 (2015).

[36] N. Zhou, L. P. Chen, Z. K. Huang, K. W. Sun, Y. Tanimura, Y. Zhao, J. Phys. Chem. A. **120**, 1562 (2016).

[37] H. Frölich, Proc. R. Soc. London **215**, 291 (1952); Adv. Phys. **3**, 325 (1954).

[38] T. Holstein, Ann. Phys. (N.Y.) **8**, 325 (1959); **8**, 343 (1959).

[39] P. A. M. Dirac, Proc. Cambridge Philos. Soc. **26**, 376 (1930); J. Frenkel, *Wave Mechanics* (Oxford University Press, 1934).

[40] C. Itzykson and J. Zuber, *Many-Particle Physics* (McGraw-Hill, 1980).

[41] O. Bramley, C. Symonds and D. V. Shalashilin, J. Chem. Phys. **151**, 064103 (2019).

[42] L. Chen, Y. Zhao, and Y. Tanimura, J. Phys. Chem. Lett. **6**, 3110 (2015).

[43] J. Sun, B. Luo and Y. Zhao, Phys. Rev. B. **82**, 014305 (2010).

[44] Z. K. Huang, L. Wang, C. Q. Wu, L. P. Chen, F. Grossman and Y. Zhao, Phys. Chem. Chem. Phys. **19**, 1655 (2017).

[45] J. F. Yu, C. Q. Wu, X. Sun, and K. Nasu, Phys. Rev. B. **70**, 064303 (2004).

[46] A. A. Bakulin, S. E. Morgan, T. B. Kehoe, M. W. Wilson, A. W. Chin, D. Zigmantas, D. Egorova, A. Rao, Nat. Chem. **8**, 16 (2016).

[47] R. Tempelaar, D. R. Reichman, J. Chem. Phys. **146**, 174703 (2017).

[48] R. Tempelaar, D. R. Reichman, J. Chem. Phys. **146**, 174704 (2017).

[49] S. Mukamel, *Principles of Nonlinear Optical Spectroscopy* (Oxford University Press, USA, 1995).

[50] T.D. Huynh, K. Sun, M. F. Gelin, Y. Zhao, J. Chem. Phys. **139**, 104103 (2013).

[51] K. W. Sun, M. Gelin, V. Chernyak and Y. Zhao, J. Chem. Phys. **142**, 212448 (2015).